Modeling of Microfluidic Fuel Cells With Flow-Through Porous Electrodes

Conference Paper · December 2010

DOI: 10.1115/FuelCell2010-33220

2 authors, including:

Ali Ebrahimi Khabbazi
Advanced Micro Devices
12 PUBLICATIONS **196** CITATIONS

SEE PROFILE

Journal of Power Sources 195 (2010) 8141–8151

Contents lists available at ScienceDirect

Journal of Power Sources

journal homepage: www.elsevier.com/locate/jpowsour

Numerical study of the effect of the channel and electrode geometry on the performance of microfluidic fuel cells

A. Ebrahimi Khabbazi, A.J. Richards, M. Hoorfar*

University of British Columbia Okanagan, Kelowna, V1V 1V7 BC, Canada

ARTICLE INFO

Article history:
Received 4 June 2010
Received in revised form 26 June 2010
Accepted 28 June 2010
Available online 24 July 2010

Keywords:
Microfluidic fuel cell
Numerical modeling
Electrochemical reaction
Polarization curve
Fuel utilization
COMSOL Multiphysics

ABSTRACT

Using COMSOL Multiphysics 3.5, 3D numerical models of different microfluidic fuel cells have been developed in this paper to determine the effect of different modifications which have been implemented in the microfluidic fuel cell since its advent. These modifications include the channel geometry aspect ratio and electrode configuration, the third flow between the anolyte and catholyte in the channel (i.e., multi-stream laminar flow), and multiple periodically placed inlets. To be consistent with the convention, the output power of the device is normalized by the electrode surface area; however, the power density calculations are also performed through normalization by the device volume. It is shown that the latter method is more realistic and providing more information from the design point of view since the ultimate goal in designing the microfluidic fuel cell is to fabricate a compact, yet powerful device. Finally, a novel design of the microfluidic fuel cell with a tapered channel is suggested and compared to the non-tapered geometry through the polarization curves. The steps which have been taken in COMSOL to obtain these polarization curves are clearly and thoroughly explained. The Butler–Volmer equation was implemented to incorporate for the electrochemical reactions at the electrodes. The "Conductive Media DC" module, in COMSOL, is used to model the electric fields within the fuel cell. The concentration distributions of the reactant species are obtained using the "Incompressible Navier–Stokes" and "Convection and Diffusion" modules. Solving these equations together predicts the current density for given cell voltage values. The results demonstrate the cell voltage losses due to activation, ohmic and concentration overpotentials. It is shown that for a fixed value of the cell voltage (say 0.45 V), the fuel cell with multiple periodically placed inlets has the highest fuel utilization (i.e., 62.3%); while the "Simple square" geometry depicts 13.8% fuel utilization at this potential. Thus, the multiple-inlets design is particularly suitable for low-voltage applications which require high current. Also, the results of the tapered geometry proposed in this paper show that tapering the channel enhances the polarization curve comparing to the square cross-section geometry with extended electrodes. In essence, the fuel utilization of the "Extended square" geometry is increased from 15.4% to 57.6% by tapering the channel. This is due to the fact that the mixing region growth rate is restricted in the tapered geometry, and hence the electrodes on the top and bottom walls of the channel can be more extended toward the centre of the channel before the crossover occurs.

1. Introduction

Recently, there has been a growing demand for small but high power sources of energy for portable devices which are expected to function for long periods of time without the need for recharging [1] (such as global positioning systems, laptops and mobile phones). The current battery technology can hardly keep up with this growing power demand [2]. A recent comparison between Li-ion batteries and fuel cells has shown that the latter has much higher power density, and hence more potential to respond to the future market [2]. Since the reactions in fuel cells are surface based, miniaturization of fuel cells, which increases the surface-to-volume ratio, leads to even further improvements in the power density [3,4]. Thus, miniaturized fuel cells are capable of bridging the gap between the battery technology and the high power density required for the portable applications. A prodigious amount of research has been conducted on the miniaturization of the conventional fuel cells [5–7]. Although the energy density of the miniaturized fuel cell increases as its size continues to shrink, several technological and mechanical challenges (e.g., issues related to water and heat management, the ohmic overpotential caused by the membrane, and machining of the graphite bipolar plates) still remain [6,8]. These challenges limit the further decrease in the size, and hence

* Corresponding author at: School of Engineering, University of British Columbia Okanagan, 3333 University Way, Kelowna, V1V 1V7 BC, Canada.
Tel.: +1 250 807 8804; fax: +1 250 807 9850.
E-mail address: mina.hoorfar@ubc.ca (M. Hoorfar).

0378-7753/$ – see front matter.
doi:10.1016/j.jpowsour.2010.06.094

Nomenclature

A	cross-sectional area of the charge transfer
D	diffusion coefficient
$E_{REVERSIBLE}$	reversible potential
F	Faraday constant
H	height of the channel
R	universal gas constant
R_f	ohmic resistance for ionic transport
S	consumption rate of reactant species
T	cell temperature
U	average flow velocity
ai_0	exchange current density
c	local concentration of the reactants
d	distance between the anode and cathode
e	mole number
i	rate of the electrochemical reaction
n	number of electrons transferred in the reaction
p	pressure
v	velocity
x	distance fluid travels down the channel
α	charge transfer coefficient
δ	inter-diffusion region width
η	activation overpotential
μ	viscosity
ρ	density
σ	ionic conductivity
ϕ_e	local potential in the electrolyte
ϕ_s	solid phase voltage

limit the increase in the power density of the miniaturized fuel cells.

Recently, a novel design and structure of the fuel cell, called the microfluidic fuel cell, has been introduced to overcome the above limitations of the miniaturized fuel cells. Fig. 1 presents the schematic of a typical Y-shaped microfluidic fuel cell. In such systems, the fuel and oxidant are introduced into a microchannel through separate inlets and form a side-by-side co-laminar flow between the electrodes, which are typically positioned along the channel. Laminar flow maintains separation of the fuel and oxidant. This eliminates the need for the membrane and overcomes the membrane-related issues (such as the ohmic overpotential and water management) mentioned for the miniaturized fuel cells. Due to the laminar nature of the flow in these systems, the transport phenomenon is diffusion limited, and hence the channel geometry plays an important role. As the fuel and oxidant streams travel down the channel the inter-diffusion region (i.e., mixing region) is established and grows due to the transportation of reactants from their own side to the other side through diffusion. This mixing region limits the amount of the reactants that can be potentially

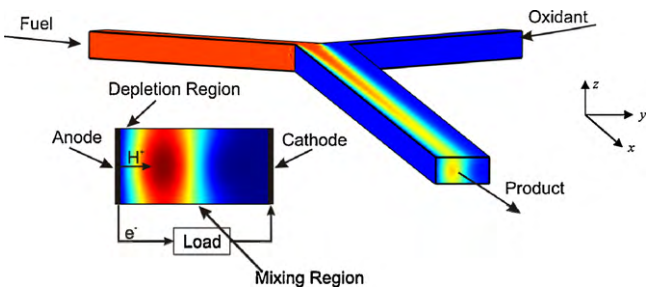

Fig. 1. A schematic of a typical Y-shaped microfluidic fuel cell.

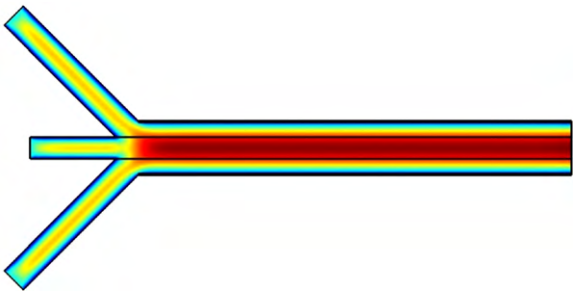

Fig. 2. A schematic of a microfluidic fuel cell with the third electrolyte stream (this schematic shows the velocity field in the microfluidic fuel cell).

available to the electrodes. This will also limit the extension of the electrodes from the wall toward the middle of the channel (which is desirable since it increases the active surface area) due the crossover issue [1]. At the same time, there is a concentration boundary layer forming on each electrode as the fluid is traveling toward the end of the channel. This concentration boundary layer (also known as depletion layer) is acting as a resistance for the reactants to reach to the active surfaces. It is desirable to have a thin depletion layer all over the electrodes.

Bazylak et al. [1] examined three different channel cross-sections with different aspect ratios, obtained the fuel and oxidant distribution, and calculated the fuel utilization. They found that the rectangular cross-sections have higher fuel utilization compared to the square ones. Chang et al. [9] also conducted a numerical analysis for a fixed flow rate and a fixed channel cross-section aspect ratio (i.e., height to width ratio). They reported that the reduction of cross-sectional area results in higher fuel cell performance. They also observed that for a constant cross-sectional area, the high aspect ratio results in a higher cell performance. The improved performance can be associated with two facts: (1) the higher the channel height, the higher the Peclet number (i.e., $Pe = UH/D$ which represents the convective to diffusive transport). The higher the Peclet number the faster the depletion regions are filled with fresh reactants, so higher current is produced by the cell; (2) in high aspect ratio geometries, the anode and cathode electrodes are closer to each other; therefore, the resistance to proton transfer in the electrolyte (Eq. (1)) is reduced [10]:

$$R_f = \frac{d}{\sigma A} \tag{1}$$

In this equation, R_f is the ohmic resistance for ionic transport, d represents the distance between the anode and cathode, σ refers to ionic conductivity and A is the cross-sectional area of the charge transfer.

Besides the channel aspect ratio and the electrode configurations, there have been a few more geometrical modifications suggested over the past few years [1,11–13]. For instance, Sun et al. [11] proposed a multi-stream laminar flow microfluidic fuel cell which is basically the same as a typical membraneless Y-shaped microfluidic fuel cell except with three inlets. Fig. 2 presents this design. The third stream is inserted between the fuel and oxidant streams to keep the anolyte and catholyte separated as they travel down the channel. The effect of inserting the third flow is similar to reducing the width of the channel, as it presses the concentration boundary layers against the electrodes which are on the side walls. This speeds up the electrochemical reactions since these reactions are a function of concentration gradient at the electrodes. In addition to the above advantage, the overall ionic resistance between the anode and cathode can be decreased if the third stream electrolyte has high proton conductivity (e.g., changing the sulfuric acid concentration in the third electrolyte affects its ionic conductivity).

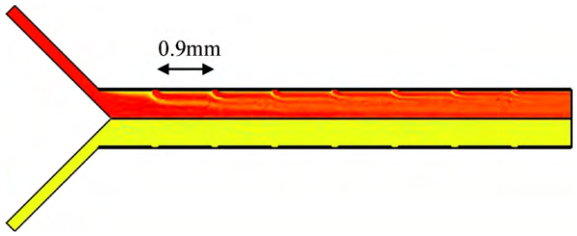

Fig. 3. A schematic of a microfluidic fuel cell with multiple periodically placed inlets (this schematic shows the concentration of the oxidant which is entering from the top side wall of the cell).

Another modification in the literature is the work of Yoon et al. [12] which suggests adding reactants through multiple periodically placed inlets to enhance the overall fuel cell performance. In this design (shown in Fig. 3), the objective is to enhance the power output by keeping the concentration gradient almost constant and high everywhere from the beginning to the end of the electrodes.

The modifications mentioned above require extensive and difficult experimental studies which are conducted to design and obtain high performance and efficient microfluidic fuel cells. The effort to design an innovative cell can be significantly reduced by developing an accurate numerical model monitoring the cell performance as modifications are added to the original design. The development of an accurate model capturing the phenomena occurring in this system, however, is not a trivial task. This paper presents, 3D numerical simulation developed using the COMSOL Multiphysics toolbox to determine the performance of different microfluidic fuel cell designs. The developed model describes the effects of activation, ohmic and mass transport overpotentials. To verify the accuracy of the simulation, first it is used to develop a model for a 30-mm long channel for which the formulations are similar to those reported by Chang et al. [9]. The two models were compared. Fig. 4 shows this comparison. It is clear that the results of the presented model in this paper are in a very good agreement with those reported before [9].

To verify further the numerical method accuracy, the results were compared to the experimental values reported by Choban et al. [14]. It is found that there is some discrepancy between the numerical results of Chang et al. [9], to which the model presented in this paper was compared, and the experimental work of Choban et al. [14] even though both studies used the same cell geometry and concentrations of fuel and oxidant species. The discrepancy is quantitative but the pattern of the polarization curves

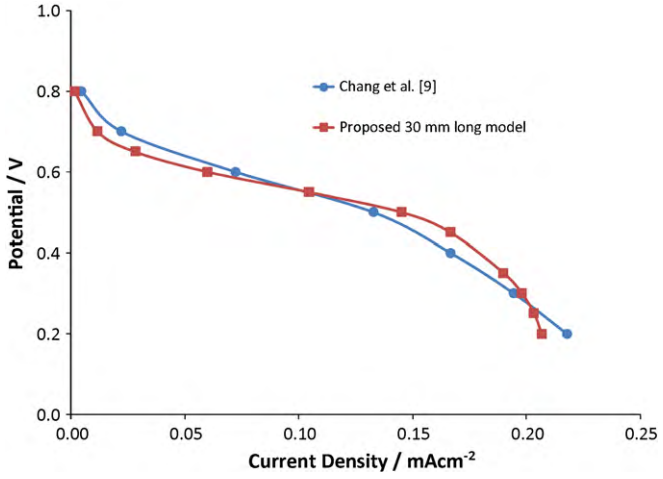

Fig. 4. . Verification of the proposed model against the results reported by Chang et al. [9] for a 30-mm long channel.

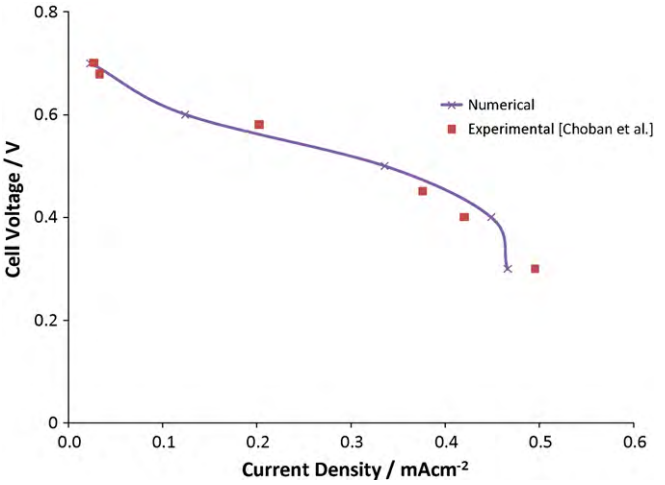

Fig. 5. Verification of the proposed model against the experimental results reported by Choban et al. [14].

is similar. To find a better agreement between the numerical values and the experimental data, it was necessary to make some adjustments to the model parameters. This issue was in part resolved by increasing the diffusion coefficient of the fuel and oxidant from 8.3×10^{-10} m^2 s^{-1} to 2.456×10^{-9} m^2 s^{-1} (this value was used by Chen et al. [15]). As another adjustment, the cathode exchange current density (a parameter related to the electrochemical activity of the oxidant species on the cathode catalyst) was doubled from 100 A m^{-3} to 200 A m^{-3}. It is reasonable to use the exchange current density as a fitting parameter since the true value is not known and depends on several factors including CO poisoning of the catalyst [1], orientation of the platinum crystals [1], and surface roughness of the electrodes [9]. Fig. 5 is obtained after making the aforementioned adjustments to the model parameters, and it shows good agreement between the calculated polarization curve and the experimental results obtained from Ref. [14]. Since the equations implemented in this model accurately describe the physics governing microfluidic fuel cell operation, the developed model can be used to fit any experimental results. Fitting the model results to match experimental data is only a matter of adjusting some of the constant parameters, such as the diffusion coefficient (as it depends on the type of the fuel/oxidant used) and the exchange current density (as it, in fact, changes from one experiment to the other experiment even if they are using the same reacting species since the orientation of the platinum crystals and surface roughness of the electrodes can be different from one experiment to another one).

Once the model was found to be in good agreement with both previous numerical and experimental values, it is used to study the effect of modifications proposed in the literature [1,9,11–13] as well as to design a new microfluidic fuel cell structure with higher performance. For this purpose, the fuel cell parameters such as Peclet number, exchange current density, diffusivity, density and viscosity of the fuel and oxidant are obtained from Chang et al. [9]. Instead of 30-mm long channel (presented in Fig. 4), which requires running the simulation for relatively long (approximately 10 h), an 8-mm long channel is used in this study to make the modeling time efficient without influencing the ultimate objective which is to study the effect of different geometries and structures of the microfluidic fuel cell on its final power output.

The details (including the governing equations and the boundary conditions) of the simulation presented here are explained in Section 3 after introducing the geometries considered in Section 2. The 3D model is used to study the effect of modifications mentioned above in the cell performance. These results are presented

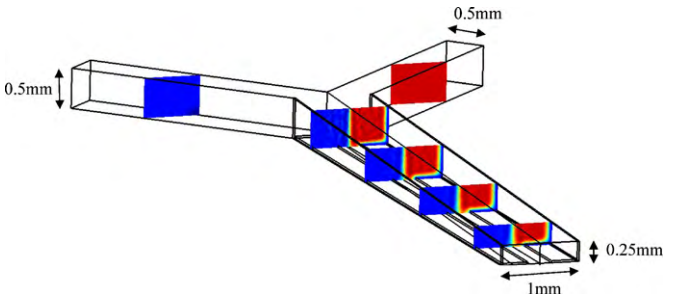

Fig. 6. A schematic of a microfluidic fuel cell with tapered channel (this figure shows the oxidant concentration profile in the lower half of the channel in different cross-sections along the channel).

in Section 4. In addition to study the effect of the modifications introduced in the literature [1,9,11–13], the model presented in this paper is also used to design a new microfluidic fuel cell structure which includes a tapered channel. In this design, the channel height is incrementally reduced from 1 mm in the beginning to 0.5 mm at the outlet. This innovative geometry is suggested based on the physical phenomena such as the development and the growth rate of the mixing region (where the fuel and oxidant meet as the anolyte and catholyte travel down the channel). The growth rate of this mixing region depends on the channel height, so the channel height can incrementally be reduced from the inlet to the outlet (i.e., the tapered geometry) to restrict the mixing (inter-diffusion) region growth rate along the channel. This will allow for the extension of the electrodes on the top and the bottom of the channel more toward the middle as the mixing region is thinner in the tapered case. The schematic of this new design is presented in Fig. 6. This figure shows only the lower half of the cell. For the numerical modeling, the channel is bisected in height to reduce the memory requirement for running the simulation. It is shown that this design incorporates higher electrode surface area inside the microchannel (compared to a non-tapered one), and hence leads to a higher-performance fuel cell. As it has been mentioned above, this new design restricts the rate of the growth of the mixing region based on the following expression [16,17]:

$$\delta \approx \left(\frac{DHx}{U}\right)^{1/3} \tag{2}$$

In this relationship, δ represents the inter-diffusion region width, x is the distance fluid travels down the channel, D, H and U are the diffusion coefficient, height of the channel and the average flow velocity, respectively. The above expression implies that by reducing the channel height (which automatically contributes to increase in U) the growth of the mixing region is limited as the fluid travels down the channel. Thus, the channel can be extended further since the diffusion region growth rate is reduced and the crossover happens farther from the inlets. This will also result in the enhancement of fuel utilization. Alternatively, the channel length can be kept constant, and the anode and cathode electrodes can be extended more toward the centre of the channel. The parts of the electrodes which are closer to the inlets are more important in terms of their contribution in power generation. Therefore, it is preferred to incorporate more electrode surface area at the beginning rather than at the end of the channel. Information on the performance of this new design is presented in Section 4.

2. Geometry

This section presents the microfluidic fuel cell geometries considered for the numerical analysis. The basic geometry is comprised of a Y-shaped channel with 1 mm × 1 mm square cross-section and 0.5 mm × 1 mm inlet cross-sections. Fig. 7 depicts the different channel cross-section aspect ratios and electrode configurations. In addition to the channel geometry and electrode configuration, the performance of the multi-stream laminar flow geometry introduced by Sun et al. [11] is also studied. This design is basically the same as the original Y-shaped geometry except it consists of an extra inlet which its width is 0.4 mm. Also, the modification introduced by Yoon et al. [12] is studied in terms of the cell performance as well as fuel utilization. This cell (see Fig. 3.) includes multiple periodically placed inlets. Although the number of inlets is increased (one main inlet and 7 minor inlets for each side), the total flow rate of the multiple-inlet cell including the injected streams and simple two-inlet cells is the same. In other words, the total inlet flux is kept fixed and equal to the other modified structures shown before to ensure the performance improvement is only due to the geometrical modification not because of the possible added flow rate. The width and the velocity of the main inlets are reduced to 0.2 mm and 0.005 m s^{-1}, respectively. The width and the velocity of the minor inlets are set to 0.114 mm and 0.00394 m s^{-1} to keep the total inlet flux consistent with the other designs. The total flow rate (250 μl min^{-1}) which is continuous consists of the flow rate from the main inlet (60 μl min^{-1}) and the flow rates (7× 27.1 μl min^{-1}) from the minor

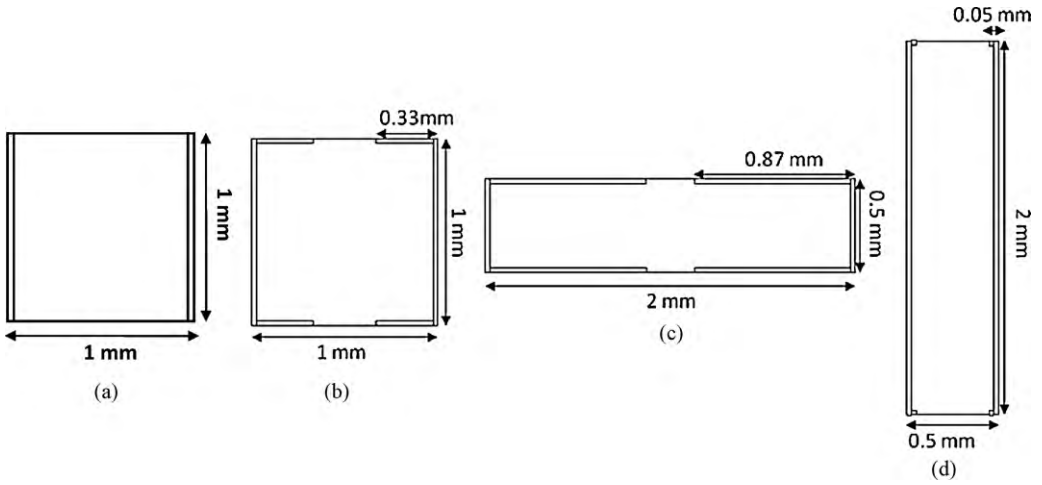

Fig. 7. The schematics and dimensions of different cross-section aspect ratios and electrode geometries are presented in (a)–(d) which are referred to a the "Simple square", "Extended square", "Low aspect ratio" and "High aspect ratio", respectively. The electrodes in (b)–(d) are extended away from the side walls toward the centre of the channel up to the edges of the mixing region.

Table 1
Constants used in the anodic and cathodic flows.

Parameter	Anode	Cathode
Flow rate	250 μl min^{-1}	250 μl min^{-1}
Density, ρ	1000 kg m^{-3}	
Dynamic viscosity, μ	0.001 Pa s	
Faraday constant, F	96,485.34 C mol^{-1}	
Cell temperature, T	298 K	
Universal gas constant, R	8.314 J mol^{-1} K^{-1}	
Ionic conductivity, σ	11.47 S m^{-1}	43 S m^{-1}
Diffusion coefficient, D	8.3×10^{-10} m^2 s^{-1}	8.3×10^{-10} m^2 s^{-1}
Charge transfer coefficient, α	0.5	0.5
Number of electrons transferred, n	2	4
Exchange current density, i_0	3.82×10^5 A m^{-3}	100 A m^{-3}
Inlet concentration, C_0	2100 mol m^{-3}	0.5 mol m^{-3}

inlets. The distance between these minor inlets is set to 900 μm (see Fig. 3).

3. Theory/calculations

The microfluidic fuel cells studied here use formic acid as the fuel and an aqueous solution of sulfuric acid saturated with oxygen as the oxidant. Although hydrogen is one of the best fuels for the PEM fuel cells, the safety concerns due to the high-pressure storage tank, especially in micro-scale devices, prevent its usage in the microfluidic fuel cell [18]. Besides the above-mentioned fact, it is to some extent hard for two gaseous streams to establish a side-by-side co-laminar flow with a thin mixing region in between. Also, the gaseous species have higher diffusion coefficient compared to the aqueous solutions. This leads to a very wide inter-diffusion region which particularly limits the amount of the electrode surface area that could be installed. Most of the studies [14,19,20] on the microfluidic fuel cells have also focused on the devices using liquid fuels due to their convenient storage. Methanol and formic acid are two examples of aqueous fuels which are typically used in microfluidic fuel cells due to their higher energy density compared to the gaseous ones. In this paper, formic acid has been selected as the fuel as it has been reported to be electrochemically more active compared to methanol [1]. The oxidation of formic acid and reduction of oxygen in the microfluidic fuel cells presented as

$$\begin{aligned} &HCOOH \rightarrow CO_2 + 2H^+ + 2e^- \\ &O_2 + 4H^+ + 4e^- \rightarrow 2H_2O \end{aligned} \tag{3}$$

3.1. Governing equations

In order to predict the effect of activation, ohmic, and concentration overpotentials on fuel cell performance, a set of steady-state conservation equations is used to model fuel cell operation. The values of various parameters used in the model are given in Table 1.

3.1.1. Fluid flow

Microfluidic flows are characterized by low Reynolds numbers due to the small dimensions of microchannels and low fluid velocities. For this reason, the flow is expected to be laminar and can be assumed to be incompressible. Also, in a typical micro-scale flow, the body forces such as the fluid weight are dominated by surface forces such as viscous shear stress. Applying mass and momentum conservation in a differential form allows the velocity field to be described by the Navier–Stokes and continuity equations [21]:

$$\begin{aligned} &\nabla \cdot v = 0 \\ &\rho(v \cdot \nabla v) = -\nabla p + \mu \nabla^2 v \end{aligned} \tag{4}$$

In these equations, v and p are the velocity and pressure, respectively. ρ and μ represent the density and viscosity which both are assumed to be equal for the two streams and constant over the whole domain. These equations can be implemented using the steady-state, laminar "Incompressible Flow" module of COMSOL Multiphysics. The flow was assumed to continue into the electrode subdomains. The no-slip boundary condition was applied to all of the channel walls. At the symmetry plane defining the top or bottom of the model geometry, a symmetry boundary was applied. A constant velocity was applied to the inlets, and the outlet was assumed to discharge to the atmospheric pressure.

3.1.2. Charge conservation

Since both the fuel and oxidant are dissolved in acidic electrolyte, the concentration of hydrogen ions was assumed to be uniform throughout the channel. Transport of protons from the anode to the cathode is by electric migration only. In these circumstances the transport of charged species and the electric field within the electrolyte can be modeled using the potential equation from the "Conductive Media DC" module of COMSOL Multiphysics. The equation describing the electric field within the electrolyte is given as

$$\sigma \nabla \cdot \nabla \phi_e = 0 \tag{5}$$

where ϕ_e is the local potential in the electrolyte. Electric insulation boundary conditions were applied to all of the channel surfaces. Within the electrodes, where charged species are generated or consumed, a current source is applied and the local current density is calculated by the Butler–Volmer reaction kinetics equation (see Section 3.1.4).

The "Conductive Media DC" module was again used to describe the voltage and current distributions within the solid-phase metallic electrodes:

$$\sigma \nabla \cdot \nabla \phi_s = 0 \tag{6}$$

Because the metallic electrodes and current collectors are highly conductive, a large value for conductivity (10^7 S m^{-1}) was used for this module. Applying a potential boundary condition for the outer electrode walls resulted in an essentially uniform solid phase voltage, ϕ_s, over the entire subdomain. The electric insulation boundary conditions were assigned to other boundaries.

3.1.3. Mass transport

Once the velocity field within the microchannel has been determined by the Navier–Stokes equation, it is possible to use the calculated velocity to model the mass transport phenomena. In microfluidic fuel cells, the reactant species are transported along the length of the channel by convection. However, diffusive transport in a direction transverse to the flow is necessary to replace reactant species in the vicinity of the electrodes, as they are consumed by reaction. When concentrations are sufficiently low, interactions between different solute species can be ignored and diffusion rates can be assumed to be linearly proportional to concentration gradients [1]. In this model, the system is assumed to be isothermal, and pressure differences are not large enough to influence diffusion coefficients. Implementing these assumptions allows the concentration distributions of the fuel and oxidant to be described by Fick's law [21] given as

$$\nabla \cdot (-D\nabla c + cv) = 0 \tag{7}$$

where c is the local concentration of the reactants. At the inlets, a uniform concentration is applied. At the outlet, the convective flux dominates mass transport and the concentration gradient normal to the outlet is set to zero. Since no transport is possible through the channel walls, insulation boundary conditions were assigned to all of the channel walls. Within the electrode subdomains (where the species are consumed by electrochemical reactions), a source

term is added to the above equation. This results in the following equation:

$$\nabla \cdot (-D\nabla c + cv) = \frac{e_i}{nF} i \tag{8}$$

where e represents the mole number, F is the Faraday constant, n denotes the number of electrons transferred in the reaction, and i reflects the rate of the electrochemical reaction which is calculated through Butler–Volmer equation (see Section 3.1.4).

3.1.4. Reaction kinetics

The Butler–Volmer equation describes the rate of an activation-controlled reaction, for which the rate of reaction is controlled solely by the rate of the electrochemical charge transfer process:

$$i = ai_0 \left[e^{((\alpha nF/RT)\eta)} - e^{(-(((1-\alpha)nF)/RT)\eta)} \right] \tag{9}$$

In the above equation, η is the activation overpotential. There is no concentration gradient term in the original Butler–Volmer equation; however, the Butler–Volmer reaction kinetics equation used here has been multiplied by the concentration term since the rate of the electrochemical reactions in microfluidic fuel cell is limited by mass transfer. As it has been mentioned earlier, when the concentrations are sufficiently low, interactions between different solute species can be ignored and diffusion rates can be assumed to be linearly proportional to concentration gradients. Reaction rates were assumed to be linearly proportional to reactant concentration. This added multiplication in the equation below (Eq. (10)) accounts for the effect of the concentrations on the reversible potential. In essence, the modified Butler–Volmer equation describes the local current density, i, across the electrode surface in the microfluidic fuel cell and is related to both the applied electric potential and the concentration of reactant species [9]:

$$i = ai_0 \frac{c}{c_{REF}} [e^{((\alpha nF/RT)\eta)} - e^{(-((1-\alpha)nF/RT)\eta)}] \tag{10}$$

The reactant species are consumed at a rate, S, which is proportional to the current density [9]:

$$S = \frac{e_i i}{nF} \tag{11}$$

At each electrode, it is necessary to calculate the activation overpotential which is required to overcome irreversibilities as the reaction deviates from its equilibrium state:

$$\eta = \phi_s - \phi_e - E_{REVERSIBLE} \tag{12}$$

The potentials of the solid electrode, ϕ_s, and the adjacent electrolyte, ϕ_e, are found by the solution of the potential equations (Eqs. (5) and (6)). The reversible potential, $E_{REVERSIBLE}$, was taken as a constant value which is based on the reaction Gibbs free energy change at standard conditions. Although the reversible potential varies with the local concentrations of the reactants and products in the electrolyte, the concentration term factored into the equation adequately accounts for the dependency of the reaction rate on the reactant concentration [22]. Using these three quantities the activation overpotential can be calculated.

For each point on the polarization curve, the cell voltage is taken as the solid phase potential assigned to the cathode since the anode is arbitrarily chosen as the ground. The current density is obtained in the post-processing by integrating the normal current density on the cathode boundaries and normalizing it by the channel volume to find the geometry that produces the highest power density per volume. This demonstrates which design is the most suitable as a compact power source for portable devices [23]. To be consistent with the results reported in the literature [9,11], the output current has also been normalized by the electrode surface area. The polarization curves obtained for different geometries are presented in Section 4.

3.2. Implementation in COMSOL

3.2.1. Solution procedures

The graphical user interface and pre-programmed modules of COMSOL Multiphysics allowed for efficient testing of different geometries and electrode configurations since the subdomain and boundary conditions could be rapidly created for different designs. A parametric sweep is used to calculate the current density at different cell voltages. Since the Butler–Volmer reaction kinetics expression creates bidirectional coupling between the potential and convection–diffusion equations, the two must be solved simultaneously in order to obtain an accurate solution. However, the coupling of these equations results in a set of non-linear equations for which it is difficult to obtain convergence from the COMSOL's non-linear solver. Therefore, instead of solving the modules in a coupled manner, it is recommended to solve this system of equations in an iterative manner. Below, two different implementations of the iterative solution procedure in COMSOL are elaborated in detail.

3.2.2. Stationary segregated

An iterative solution procedure was implemented by using the stationary segregated solver. This method allows for a stable solution procedure with reduced memory requirements while still accounting for the coupling between the physics modules. To keep the solution time reasonable and ensure a robust solution procedure, the direct UMFPACK linear system solver was used for all modules. The advantage of this method is that the user can determine a preferred termination criterion in terms of value of the relative error used to terminate the iterations.

3.2.3. Sequenced solver

This iterative procedure can be implemented by using a solver sequence. The fluid flow equations (Eq. (4)) can be solved first, since the solution to these equations is not influenced by the other modules in the model. The solution is then stored to describe the velocity field for the convection–diffusion equation. The coupling of the potential and convection–diffusion equations results again in a set of non-linear equations which requires an accurate initial estimate of the solution in order to obtain convergence from COMSOL's non-linear solver. To obtain this estimate, the equations are solved independently in an iterative manner. The electric field was first determined by solving the potential equations (Eqs. (5) and (6)) with the default linearization point. Using the calculated electric field and the stored solution for the velocity field, the convection–diffusion equation is solved to obtain an initial estimate of the concentration distribution. The calculated concentration distribution is used to solve the potential equation again to obtain a second estimate for the electric field which is then used to solve the second iteration of the convection–diffusion equation (Eq. (8)). After several iterations, the two equations were solved simultaneously. Tests were performed to ensure that the calculated polarization curve was independent of the number of iterations. Again, to keep the solution time reasonable and ensure a robust solution procedure, the direct UMFPACK linear system solver was used for all modules.

Both above methods have been tested for a few points. They both gave almost the same results. In this paper, however, the first method (i.e., stationary segregated) was used to determine the relative error as a termination criterion.

3.3. Meshing

It was found that a very fine mesh pattern was required around the electrodes to obtain convergence and ensure that the solution is accurate and independent of the mesh size. This refinement was

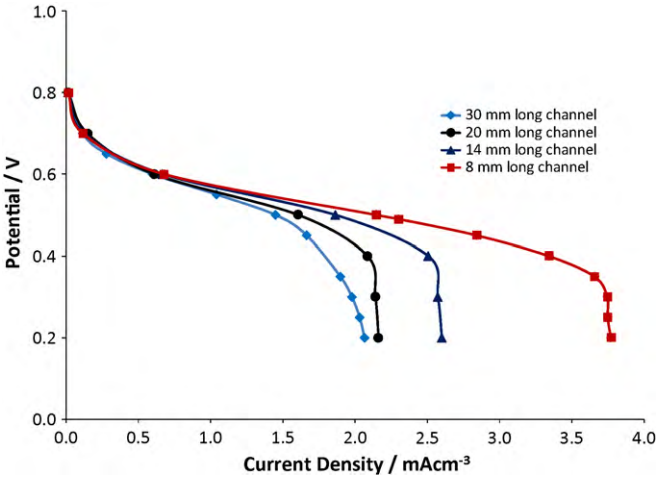

Fig. 8. The effect of the channel length on the microfluidic fuel cell performance.

made for two reasons: (1) to allow for computing the accurate flux when calculating the current density, and (2) to ensure the numerical stability of the convection–diffusion equation which can become unstable in the presence of steep concentration gradients.

The model was solved on a 64-bit Windows Vista platform, with an Intel Xeon 2.26 GHz quad-core processor. Peak memory usage was observed to be about 5 GB.

4. Results and discussion

Cell polarization curves are used as a quantitative measure for cell performance. In previous studies [9,11,13,16,18], the current and power were conventionally normalized by the electrode surface area. However, it is reasonable to normalize the current and power by the overall fuel cell volume, which is the most clear indication of the fuel cell's effectiveness as a compact power source [23]. For most of the polarization curves obtained here, normalizing based on the volume or area does not change the final results. For these cases, the polarization curves obtained based on normalizing the current by the volume are only presented. In the case(s) in which the outcome depends on which normalization is used, both types of polarization curves (per unit volume and area) are presented.

The model explained in the previous section was first used to study the effect of the length of the channel on the cell performance. The results of this study are presented in Fig. 8. It is clear that by reducing the channel length higher power densities can be achieved. This is due to the fact that the concentration boundary layer is thinner at the beginning of the channel. The thinner the boundary layer, the higher the concentration gradient. Higher concentration gradient leads to higher reaction rates which finally results in higher current generation. As the fluid travels down the channel, the boundary layer becomes thicker, and hence the concentration gradient becomes smaller which slows down the reaction rate. As a result, the electrode surface area at the vicinity of the inlets is more crucial in terms of power generation. That is why shorter channel contributes to higher power density. There is one problem associated with the short-length channels and that is low fuel utilization, which is defined as the ratio of the amount of the consumed species at the electrodes to the total amount of the fuel delivered to the cell (Eq. (13)). This problem can be alleviated by fuel circulation [18].

$$\text{fuel utilization} = \frac{\langle c\vec{u}\rangle_{inlet} - \langle c\vec{u}\rangle_{outlet}}{\langle c\vec{u}\rangle_{inlet}} \quad (13)$$

where $\langle c\vec{u}\rangle$ represents the concentration flux.

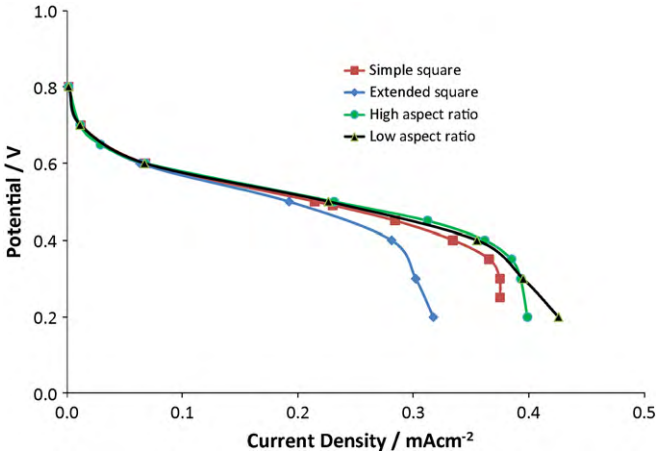

Fig. 9. The effect of the channel aspect ratio and electrode geometry (the current is normalized by the surface area).

Fig. 9 compares the polarization curves obtained for microfluidic fuel cells with different cross-section aspect ratios (i.e., height to width ratio). The results presented in Fig. 9 were obtained based on normalization of the current by the surface area. One of the important points in Fig. 9 is regarding to the "Extended square" configuration which is basically the square cross-section with the electrodes extended away from the side walls toward the centre of the channel up to the edges of the mixing region (see Fig. 7(b)). When the results are presented based on normalizing the current by the surface area, the performance of the cell with the "Simple square" cross-section seems to be better than that of the "Extended square" cross-section. It may seem that the added surface area by extension of the electrodes toward the centre of the channel does not contribute to current generation as much as the side wall electrodes do. However, this comparison still leaves some uncertainty as to which is a better design because the larger electrode area of the "Extended square" design may compensate for the lower per area output. Normalizing by volume removes this uncertainty and shows conclusively that the greater active area of the "Extended square" geometry does in fact compensate for the lower per area performance, and is actually a better design from the point of view of developing a compact power source (see Fig. 10). The fuel utilization of these geometries is also obtained. It is found that the fuel utilization for the "Simple square" and the "Extended square" geometries at 0.45 V is 13.8% and 15.4%, respectively.

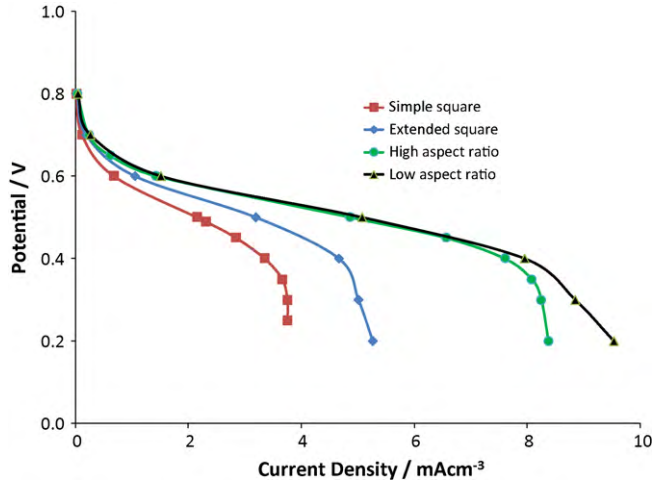

Fig. 10. The effect of the channel aspect ratio and electrode geometry (the current is normalized by the cell volume).

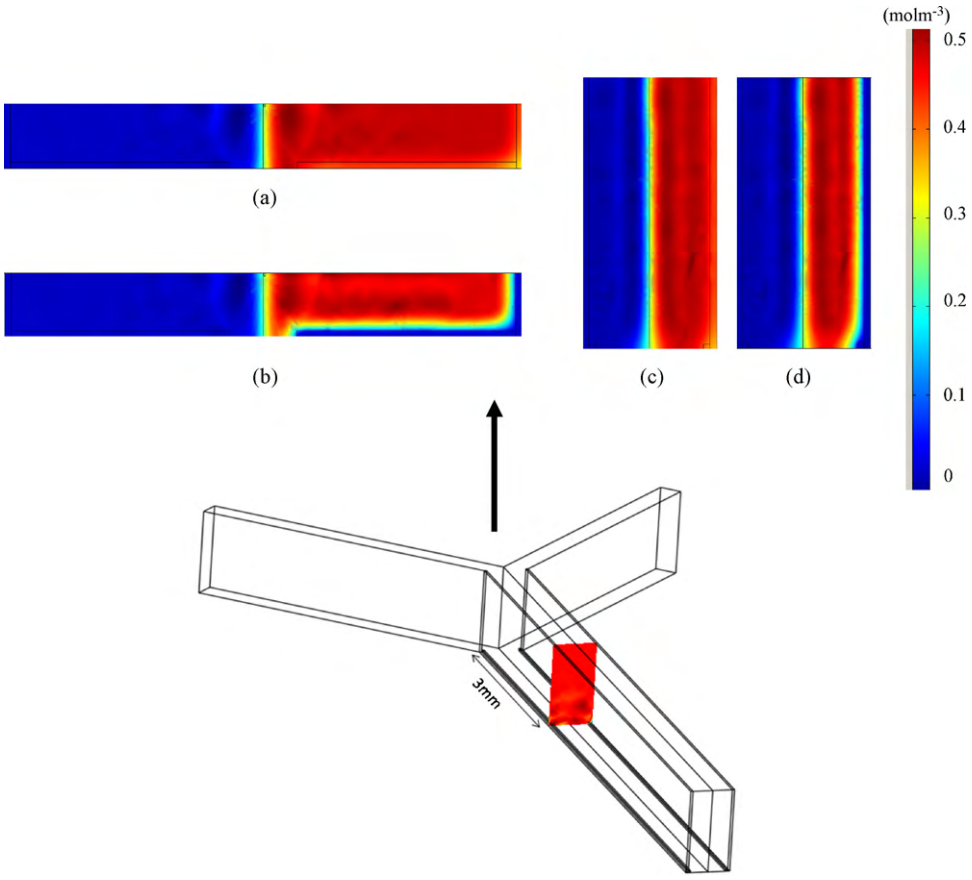

Fig. 11. Oxidant concentration contour plot at two different cell voltages (600 mV and 320 mV) emphasizing on the loss of oxidant at the vicinity of the electrodes (depletion regions) particularly in (b) "Low aspect ratio" operating at 320 mV and (d) "High aspect ratio" operating at 320 mV. (a) and (c) The oxidant concentration at 600 mV.

The high and low aspect ratio geometries have higher power density than the square channels for both area- and volume-based normalization (see Figs. 9 and 10). This is due to the high electrode surface area incorporated in these designs (see Fig. 7(c) and (d)). The active surface area in the "Low aspect ratio" geometry is 4.48 mm × 8 mm which is slightly more than what is incorporated in the "High aspect ratio" geometry (i.e., 4.2 mm × 8 mm). In spite of the above fact, both geometries have approximately the same power output up to a certain point in the polarization curve. This is because of the high Peclet number and low average ionic resistance of the electrolyte in the "High aspect ratio" geometry compared to those in the "Low aspect ratio" geometry. These two factors compensate for the slightly smaller active surface area in the "High aspect ratio" geometry, and hence cause the "High aspect ratio" design to generate almost the same power output as the "Low aspect ratio" structure for low to medium range of current densities. At very high current densities, the main limiting factor is the mass transport issue which is caused by the loss of reactants at the vicinity of the electrodes (and low rate of species diffusion). The concentration of the oxidant around the cathode for low and high aspect ratio geometries is shown in Fig. 11. This mass transport issue dominates over the ohmic losses making the available electrode surface area a more important parameter in current generation compared to the overall ionic conductance between the anode and cathode. Therefore, from a certain point onward, the lower ionic resistance of the "High aspect ratio" design cannot compensate for its lower electrode surface area as the active surface area is more important factor compared to the ionic conductance in high current densities. In other words, it is easier for the reacting species to reach to the active sites when the electrode surface area is larger. In the "Low aspect ratio" channel the larger active surface area alleviates the mass transport issue to a certain extent and prevents the sharp drop of the polarization curve similar to what is observed for the "High aspect ratio" geometry at high current density region.

The relative importance of the active surface area at high current densities as opposed to low current densities can also be understood by examining the relationship between mass transport and current generation and studying the concentration gradient around the electrodes for different points on the polarization curve (one at low and the other at high cell voltage). Since it is a diffusive process, the mass transport from the bulk flow to the electrodes is directly dependent on concentration gradients. Neglecting the two small boundaries at the start and end of the electrode subdomains, the total concentration flux of the reactant entering either the anode or cathode can be calculated by integrating the concentration gradient over the electrode boundaries as in Eq. (14):

$$\text{electrode concentration flux} = \int_s D\nabla c \cdot d\vec{A} \tag{14}$$

where $d\vec{A}$ is the differential area vector normal to the electrode surface.

Since there can be no accumulation or depletion of reactant species in steady-state operation, the consumption rate of reactant species by electrochemical reactions and the diffusive flux of reactants entering the electrode subdomains must be equal (again neglecting the small electrode boundary at the outlet where some reactant is removed from the cell by convection). Therefore, the total current generated by the fuel cell, I, which is proportional to the reactant consumption rate, must also be proportional to the concentration flux of reactant species entering the electrode

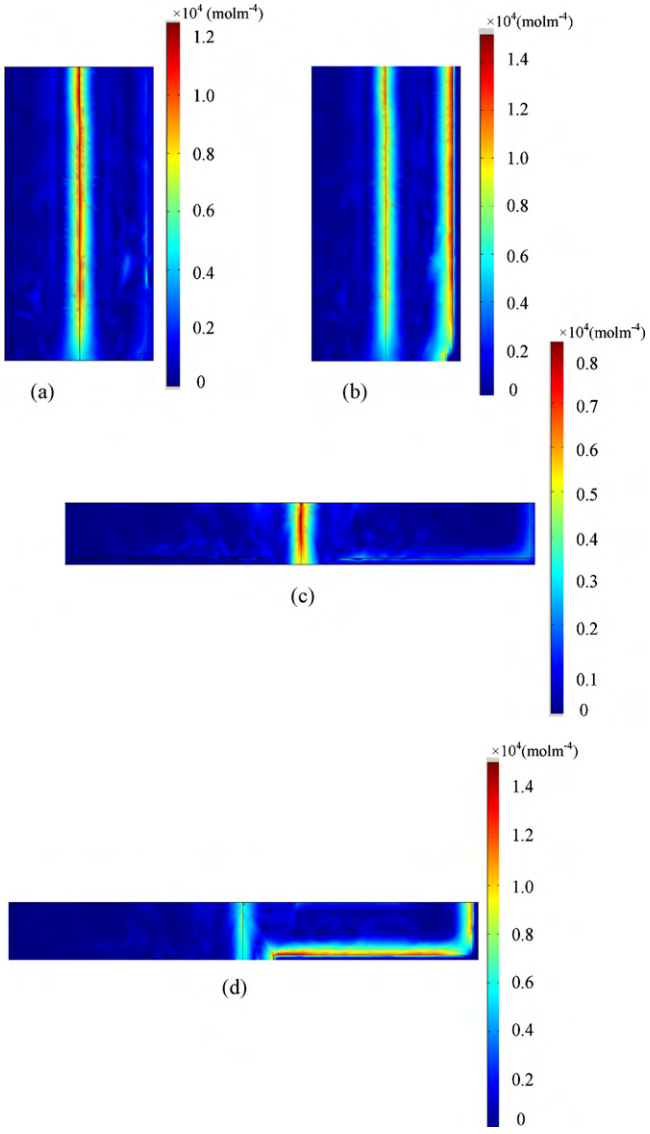

Fig. 12. Contour plots (plane at $x = 3$ mm) showing the concentration gradient of the oxidant in (a) "High aspect ratio" operating at 600 mV, (b) "High aspect ratio" operating at 320 mV, (c) "Low aspect ratio" operating at 600 mV and (d) "Low aspect ratio" operating at 320 mV.

subdomain and can be calculated as below:

$$I = \frac{nF}{e_i} \int_s D\nabla c \cdot d\vec{A} \tag{15}$$

Eq. (15) indicates that the fuel cell current is essentially proportional to the product of the concentration gradient and electrode area. Fig. 12 shows that for the same operating voltage, both the low and high aspect ratio channels have similar concentration gradients. Also, the concentration gradients for low cell voltages (corresponding to higher average current density) are greater in both cases. Since the concentration gradients for both cells are similar when operating at the same voltage, the difference in total current output is proportional to the difference in the active area. Although the relative difference in current output of the two cells will remain approximately the same for different operating voltages, the absolute difference will increase at lower cell voltages due to the multiplication of the difference in active area with greater concentration gradients. This effect is manifested in the polarization curve by the growing gap between the current density of the two cells as the operating voltage decreases.

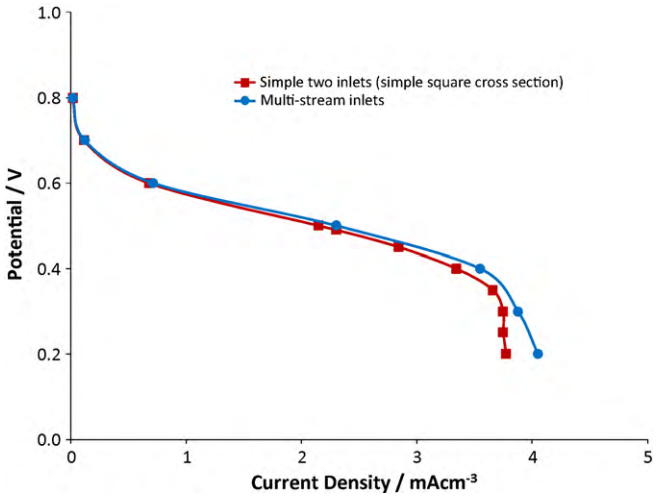

Fig. 13. The effect of inserting the third flow between the anolyte and catholyte on the polarization curve.

The fuel utilization of the low and high aspect ratio channels is also obtained. It is found that the fuel utilization for both designs is approximately 18% when the cell voltage is at 0.45 V.

As mentioned before, the model presented in this paper was also used to study the performance of the multi-stream laminar flow configuration (shown in Fig. 2). The results are presented in Fig. 13. The slight improvement in the polarization curve of the multi-stream laminar flow design is because of the steeper concentration layers and higher ionic conductivity between the anode and cathode. The electric conductivity of the diluted sulfuric acid which has been used in the third flow is assumed to be 47 S m^{-1} and the flow rate is set to 200 μl min^{-1}. The inlet velocity of the third stream was arbitrarily set to match the inlet velocities of the fuel and oxidant streams. The fuel utilization for this design is 30.07%. The higher fuel utilization of this design compared to the "Simple square" geometry is due to the fact that the concentration boundary layers are pressed to the channel walls, so the concentration gradients are higher as opposed to what it is in the "Simple square" design. In essence, the higher the concentration gradient, the faster the electrochemical reactions.

The multiple periodically placed inlets design was also modeled and compared to the standard two-inlet design. Fig. 14 presents the results. The sudden fall at high current densities in the polarization curve of the simple two-inlet design is due to the mass transfer

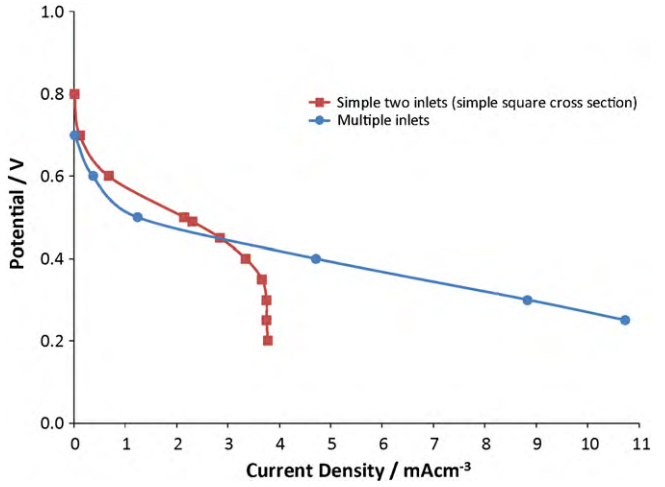

Fig. 14. The effect of multiple periodically placed inlets modification on the polarization curve.

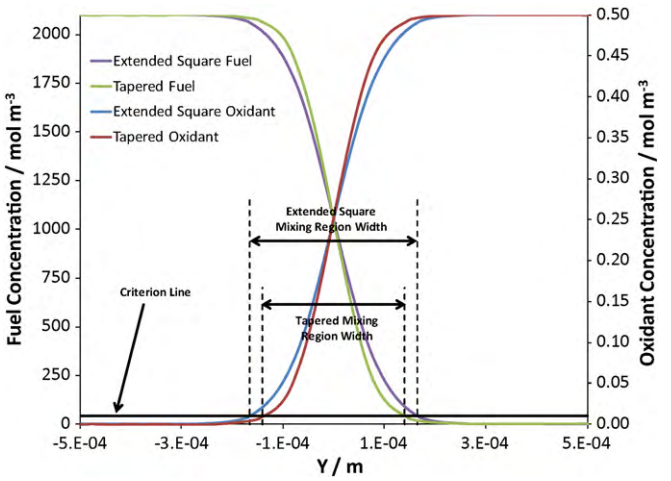

Fig. 15. A Comparison of the mixing region width in the "Extended square" and the proposed tapered geometry is shown. The criterion line indicates 2% of the maximum concentration of the fuel or oxidant which is used to define the width of the mixing region.

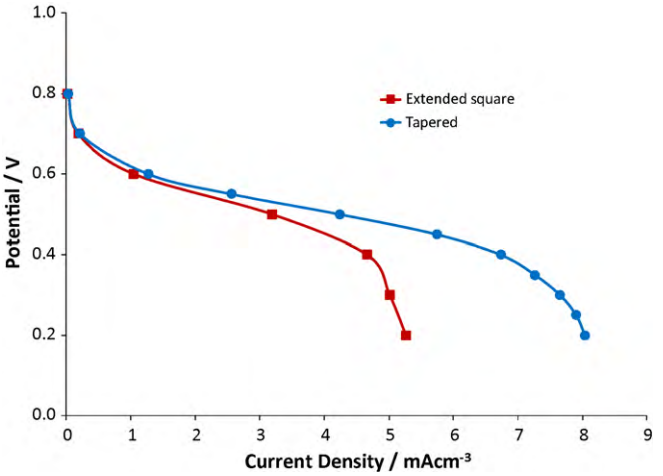

Fig. 16. The effect of tapering the channel on the polarization curve.

issue. At high current densities, the reactant consumption rate is much higher than the rate of mass transfer to the electrodes. In the multiple periodically placed inlets design, on the other hand, the depleted areas are filled with fresh reactants injected from the minor inlets along the channel, which resolves the mass transfer issue. Therefore, there is no sudden drop at high current densities. The total flow rate of this design and the simple two-inlet design is the same; therefore, the mass transport issue is resolved solely by the multiple injections to the depleted areas not by any possible added flow rates. This design turns out to be very useful for the applications in which low voltage with high current density is needed. The fuel utilization is 62.3%. This high fuel utilization is due to the fast replenishment of the depletion regions through the minor inlets.

Finally, the simulation presented in this paper was used to design a new geometry to reduce the growth rate of the width of the mixing region. By tapering the channel (i.e., incremental reduction in the channel height), the mixing region growth rate is restricted. A comparison of the mixing regions calculated by the model for the tapered design and the "Extended square" design is shown in Fig. 15. The figure shows the concentrations of the fuel and oxidant species across the width of the channels at the lower boundary of the outlet cross-section where the mixing region is at its widest extent. Since the concentration boundary layer does not influence the inter-diffusion of species across the co-laminar interface, the reaction source terms in the electrode subdomains were removed to make the simulation faster and less memory intensive, and consequently the concentration boundary layers near the electrodes are not shown. However, Fig. 15 does show that the diffusion of the fuel or oxidant species into opposite side of the channel is clearly reduced in the tapered design.

In this work, the mixing region thickness is defined as the distance over which the concentration of the fuel or oxidant falls to 2% of its maximum value. Using this definition, the mixing region in the tapered channel is found to be 0.04 mm thinner. Since the electrodes must not overlap with the mixing region in order to avoid crossover, the smaller mixing region in the tapered channel allows the anode and cathode to be extended an additional 0.02 mm toward the centre of the channel. This extension creates 0.32 mm^2 of additional anode or cathode area in the 8-mm long channel. The increased active area increases the cell current density as shown in Fig. 16. The new tapered design also enhances the fuel utilization by up to four times.

5. Conclusions

In this paper, a comprehensive numerical study has been conducted to compare the performance of the different microfluidic fuel cell designs reported in the literature (e.g., microfluidic fuel cells with different cross-section aspect ratios and electrode configurations, multi-stream laminar flow microfluidic fuel cells, and fuel cells with multiple periodically placed inlets). Polarization curves were obtained by integrating the normal current density on the cathode boundaries using COMSOL Multiphysics. The results show that changing the cross-section aspect ratio has significant impact on the cell performance. For instance, it was found that the high and low aspect ratios are better than the square one. At a very high current density (i.e., 8 mA cm^{-3} or even higher) the low aspect ratio geometry is proven to perform better; however, the high aspect ratio structure slightly performs better at lower current densities. Adding the third flow between the anode and cathode contributes to a small improvement in the polarization curve. However, it was found that implementing multiple periodically placed inlets has a great positive impact on the polarization curve. This design depicts 62.3% fuel utilization at a selected voltage value (say 0.45 V). This high fuel utilization which finally leads to high power generation (in a fixed potential) is due to the fast replenishment of the depletion area at the vicinity of the electrodes by the minor inlets.

The numerical method presented in this paper is a valuable tool, as it can be used to study the effect of any modifications on the cell performance before fabricating and testing the new design in an extensive and difficult experimental study. For instance, the model was used to design a new structure here. The proposed design includes a tapered channel which has a great impact on the polarization curve and fuel utilization. By tapering the channel it is possible to incorporate wider electrodes on the bottom and top walls of the channel before the crossover occurs. This even increases the fuel utilization up to four times.

Acknowledgements

This work was supported by the Natural Science and Engineering Research Council (NSERC) of Canada. Financial support through the NSERC Undergraduate Student Research Award (USRA) (A.J. R) is gratefully acknowledged.

References

[1] A. Bazylak, D. Sinton, N. Djilali, Journal of Power Sources 143 (2005) 57–66.
[2] C.K. Dyer, Journal of Power Sources 106 (2002) 31–34.

[3] G.F. McLean, N. Djilali, M. Whale, T. Niet, Proceedings of the 10th Canadian Hydrogen Conference, 2000, pp. 349–358.
[4] R. Hahn, S. Wagner, A. Schmitz, H. Reichl, Journal of Power Sources 131 (2004) 73–78.
[5] J. Yu, P. Cheng, Z. Ma, B. Yi, Electrochimica Acta 48 (2003) 1537–1541.
[6] S. Lee, A. Chang-Chien, S. Cha, R. O'hayre, Y. Park, Y. Saito, F. Prinz, Journal of Power Sources 112 (2002) 410–418.
[7] J. Yeom, G. Mozsgai, B. Flachsbart, E. Choban, A. Asthana, M. Shannon, P. Kenis, Sensors & Actuators B: Chemical 107 (2005) 882–891.
[8] A. Ozbek, Electronic Design 51 (2003) 102–106.
[9] M.-H. Chang, F. Chen, N.-S. Fang, Journal of Power Sources 159 (2006) 810–816.
[10] E. Kjeang, N. Djilali, D. Sinton, Journal of Power Sources 186 (2009) 353–369.
[11] M.H. Sun, G. Velve Casquillas, S.S. Guo, J. Shi, H. Ji, Q. Ouyang, Y. Chen, Microelectronic Engineering 84 (2007) 1182–1185.
[12] S.K. Yoon, G.W. Fichtl, P.J.A. Kenis, Lab on a Chip 6 (2006) 1516–1524.
[13] R.S. Jayashree, L. Gancs, E.R. Choban, A. Primak, D. Natarajan, L.J. Markoski, P.J.A. Kenis, Journal of the American Chemical Society 127 (2005) 16758–16759.
[14] E.R. Choban, L.J. Markoski, A. Wieckowski, P.J.A. Kenis, Journal of Power Sources 128 (2004) 54–60.
[15] F. Chen, M.-H. Chang, M.-K. Lin, Electrochimica Acta 52 (2007) 2506–2514.
[16] R. Ferrigno, A.D. Stroock, T.D. Clark, M. Mayer, G.M. Whitesides, Journal of the American Chemical Society 124 (2002) 12930–12931.
[17] R.F. Ismagilov, A.D. Stroock, P.J.A. Kenis, G. Whitesides, Applied Physics Letters 76 (17) (2000) 2376–2378.
[18] A. Li, S.H. Chan, N.T. Nguyen, Journal of Micromechanics and Microengineering 6 (2007) 1107–1113.
[19] S. Motokawa, M. Mohamedi, T. Momma, S. Shoji, T. Osaka, Electrochemistry Communications 6 (2004) 562–565.
[20] J. Yeom, R.S. Jayashree, C. Rastogi, M.A. Shannon, P.J.A. Kenis, Journal of Power Sources 160 (2006) 1058–1064.
[21] R.B. Bird, W.E. Stewart, E.N. Lightfoot, Transport Phenomena, 2nd ed., John Wiley, New York, 2002.
[22] S. Um, C. Wang, K. Chen, Journal of Electrochemical Society 147 (2000) 4485–4493.
[23] E. Kjeang, R. Michel, D.A. Harrington, N. Djilali, D. Sinton, Journal of the American Chemical Society 130 (2008) 4000–4006.